iScience

CellPress
OPEN ACCESS

Article

m^{6}A regulation of cortical and retinal neurogenesis is mediated by the redundant m^{6}A readers YTHDFs

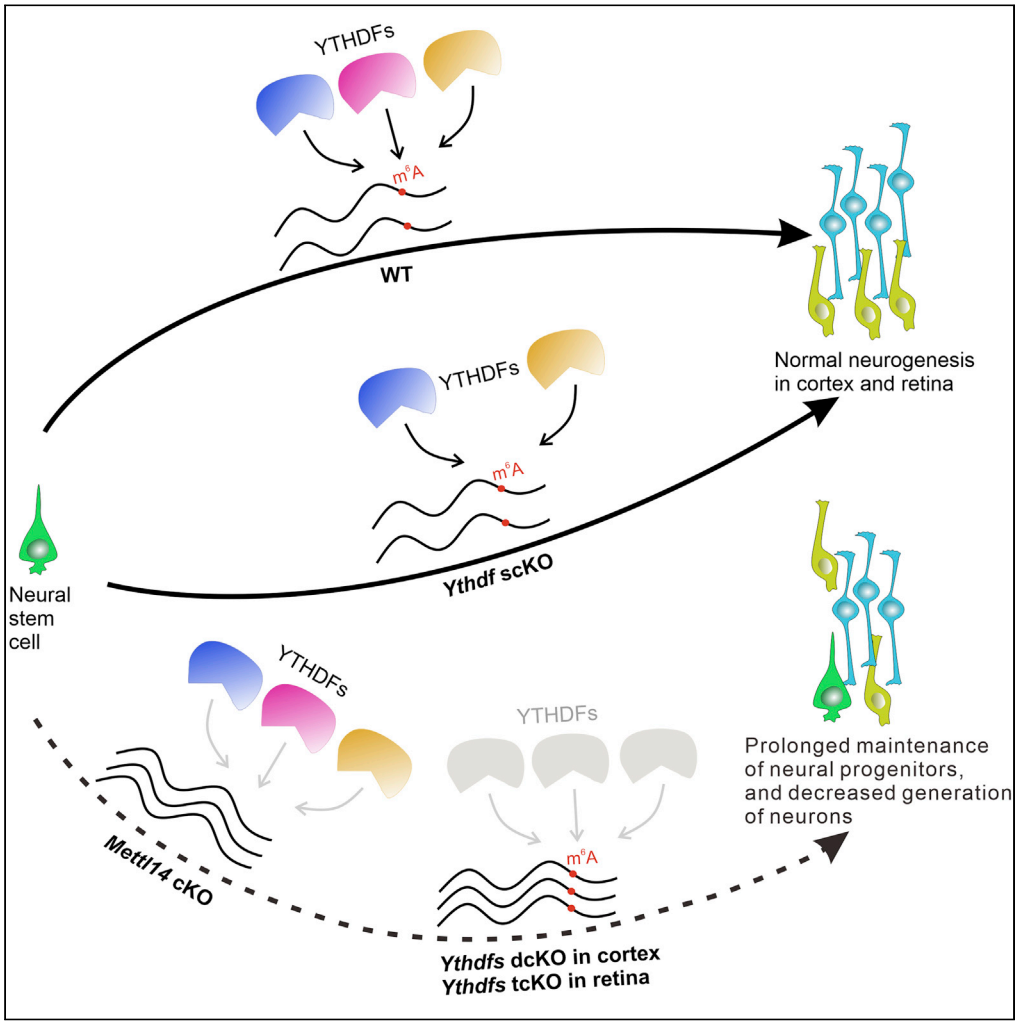

Fugui Niu, Pengfei Che, Zhuoxuan Yang, ..., Mengru Zhuang, Xijun Ou, Sheng-Jian Ji

ouxj@sustech.edu.cn (X.O.)
jisj@sustech.edu.cn (S.-J.J.)

Highlights

YTHDF1 and YTHDF2 have redundant functions in m^{6}A regulation of cortical neurogenesis

m^{6}A modification plays a critical role in retinal neurogenesis

Only *Ythdf1*, *Ythdf2*, and *Ythdf3* triple deletion disrupts retinal neurogenesis

YTHDF1 and YTHDF2 share a large pool of target mRNAs related to neurogenesis

Niu et al., iScience 25, 104908
September 16, 2022
https://doi.org/10.1016/j.isci.2022.104908

iScience

CellPress
OPEN ACCESS

Article

m^{6}A regulation of cortical and retinal neurogenesis is mediated by the redundant m^{6}A readers YTHDFs

Fugui Niu,[1,2,3,5] Pengfei Che,[2,5] Zhuoxuan Yang,[2] Jian Zhang,[2] Lixin Yang,[2] Mengru Zhuang,[2] Xijun Ou,[4,*] and Sheng-Jian Ji[2,6,*]

SUMMARY

m^{6}A modification plays an important role in regulating mammalian neurogenesis. However, whether and how the major cytoplasmic m^{6}A readers, YTHDF1, YTHDF2, and YTHDF3 mediate this process is still not clear. Here, we demonstrate that *Ythdf1* and *Ythdf2* double deletion but not individual knockout recapitulates the phenotype of *Mettl14* knockout in cortex. In addition, we find that *Mettl14* knockout in retina causes protracted proliferation of retinal progenitors, decreased numbers of retinal neurons, and disturbed laminar structure. This phenotype is only reproduced when *Ythdf1*, *Ythdf2*, and *Ythdf3* are knocked out simultaneously in retina. Analysis of YTHDF target mRNAs in mouse cortex and retina reveals abundant overlapping mRNAs related to neurogenesis that are recognized and regulated by both YTHDF1 and YTHDF2. Together our results demonstrate that the functionally redundant YTHDFs mediate m^{6}A regulation of cortical and retinal neurogenesis.

INTRODUCTION

N^6-methyladenosine (m^{6}A) modification, as the most abundant internal modification on mRNA, is dynamically regulated by its "writers" and "erasers", and recognized by its "readers" (Meyer and Jaffrey, 2017). These readers include the YTH domain-containing proteins such as YTHDF1, YTHDF2, YTHDF3, YTHDC1, and YTHDC2, and bind the m^{6}A site directly to exert multiple functions such as mRNA splicing, alternative polyadenylation, nucleus export, degradation, and translation (He and He, 2021; Zaccara et al., 2019). However, the functional relations among different YTHDFs readers remain controversial: initial studies suggested that different YTHDFs have distinct functions and working mechanisms (Shi et al., 2017; Wang et al., 2014, 2015b); later studies argued that different YTHDFs work redundantly (Kontur et al., 2020; Lasman et al., 2020; Zaccara and Jaffrey, 2020); a recent study showed that YTHDF1 and YTHDF2 could work synergistically to regulate the same pathway and process (Yu et al., 2021). Thus, further clarification is needed to elucidate the functions of YTHDFs.

Neurogenesis is the process of neural stem cell proliferation, migration, and differentiation that is precisely regulated by diverse factors and mechanisms. In neocortical neurogenesis, self-renewal radial glial cells in the ventricular zone (VZ) differentiate into the intermediate progenitors in the subventricular zone (SVZ) and then give rise to neurons that migrate into the specified cortical layers in an "inside-out" order (Fishell and Kriegstein, 2003; Woodworth et al., 2012). In retinal neurogenesis, all retinal neurons are derived from the retinal progenitors with a particular order and organized into the proper laminar structure from embryonic to postnatal stages (Cepko, 2014).

Two studies reported that deletion of the m^{6}A writer METTL14 results in severe defects in cortical neurogenesis (Wang et al., 2018; Yoon et al., 2017). However, these two studies using the same *Nestin-cre* to ablate *Mettl14* came up with two contrary mechanisms to explain their results (Wang et al., 2018; Yoon et al., 2017), suggesting that further exploration and clarification is needed to decide the role of m^{6}A modification in cortical neurogenesis. In addition, whether and how the m^{6}A readers mediate m^{6}A modification in cortical neurogenesis remain to be studied. Moreover, whether m^{6}A modification and its readers work similarly or distinctly to regulate neurogenesis in different brain regions remain elusive.

[1]Harbin Institute of Technology, Harbin, Heilongjiang 150001, China

[2]School of Life Sciences, Department of Biology, Brain Research Center, Shenzhen Key Laboratory of Gene Regulation and Systems Biology, Southern University of Science and Technology, Shenzhen, Guangdong 518055, China

[3]SUSTech-HIT Joint Graduate Program, Southern University of Science and Technology, Shenzhen, Guangdong 518055, China

[4]School of Life Sciences, Department of Biology, Southern University of Science and Technology, Shenzhen, Guangdong 518055, China

[5]These authors contributed equally

[6]Lead contact

*Correspondence: ouxj@sustech.edu.cn (X.O.), jisj@sustech.edu.cn (S.-J.J.)

https://doi.org/10.1016/j.isci.2022.104908

Here, we used *Mettl14* conditional knockout (cKO) by *Nestin-cre* and *Six3-cre* to examine the functions of m^6A modification in cortical and retinal neurogenesis, respectively. By generating single, double, or triple deletion of *Ythdf1*, *Ythdf2* and *Ythdf3*, and comparing their phenotypes with that of *Mettl14* cKO in cortex and retina, we investigated how YTHDFs mediate m^6A modification and whether they are redundant in cortical and retinal neurogenesis. Finally, we identified target mRNAs of YTHDFs. Together, our results reveal mechanisms by which the m^6A readers YTHDFs mediate m^6A modification in neurogenesis of different brain regions.

RESULTS

Mettl14 deletion delays cortical neurogenesis and reduces production of neurons

To further explore and clarify the function of m^6A modification in cortical neurogenesis, we first checked m^6A modification level in the embryonic cortex. Immunostaining with a widely used m^6A antibody revealed high m^6A level in the developing cortex (Figure S1A). Abundant m^6A modification in the radial glia cells and intermediated progenitors supports the function of m^6A modification in the cortical neurogenesis. To test this, we generated *Mettl14* conditional knockout (cKO) by crossing *Mettl14* $^{fl/fl}$ with *Nestin-cre*$^{+/-}$ to get *Nestin-cre*$^{+/-}$, *Mettl14* $^{fl/fl}$. The knockout efficiency of METTL14 protein in the cKO mouse was verified by anti-METTL14 immunostaining, which demonstrated that METTL14 was ablated successfully in the cKO mouse cortex (Figure S1B). The numbers of Pax6$^+$ radial glia cells in the ventricular zone (VZ) and Tbr2$^+$ intermediate progenitors were dramatically larger in the *Mettl14* cKO cortex compared with control at P5 (postnatal day 5) (Figures S1C–S1E). We continued to use Tbr1 to label layer VI neurons and Ctip2 to label layer V neurons (Woodworth et al., 2012). The quantification and measurement also revealed significant increase in the thickness of layers WM-SVZ-VZ including white matter (WM), subventricular zone (SVZ) composed by intermediate progenitors, and VZ made up of radial glia cells (Figures S1F and S1G). Larger numbers of radial glia cells and intermediate progenitors and thicker SVZ and VZ indicate that the maintenance of radial glia cells is abnormally extended to postnatal stages in the *Mettl14* cKO cortex. In contrast, dramatic decreases in the thickness of layers VI, V, and I–IV were observed in the cKO cortex, indicating the defects of neuron production in the *Mettl14* cKO cortex (Figures S1F and S1G). These results demonstrate that knockout of the m^6A writer METTL14 could delay cortical neurogenesis to postnatal stage and lead to defects in the production of neurons.

Ythdf1 or *Ythdf2* conditional knockout mice show no defect in cortical neurogenesis

To identify which reader(s) directly mediate functions of m^6A modification in cortical neurogenesis, we first investigated the expression patterns of YTHDF1 and YTHDF2 in the developing cortex. The co-staining of YTHDF1 or YTHDF2 with Pax6 showed YTHDF1 and YTHDF2 are highly expressed in the radial glia cells in embryonic cortex from E11 (embryonic day 11) to E13.5 (Figures 1A and 1B), suggesting an early role of YTHDFs in cortical neurogenesis. With decreases of radial glia cells, the expression of YTHDFs also show decreases from E15.5 to P0 (Figures 1A and 1B). We first generated conditional knockouts of *Ythdf1* and *Ythdf2* respectively, by crossing *Ythdf1*$^{fl/fl}$ and *Ythdf2*$^{fl/fl}$ with *Nestin-cre* to get *Nesin-cre*$^{+/-}$,*Ythdf1*$^{fl/fl}$ (*Ythdf1* scKO) and *Nesin-cre*$^{+/-}$,*Ythdf1*$^{fl/fl}$ (*Ythdf2* scKO) mice. Anti-YTHDF1 and YTHDF2 immunostaining showed that these reader proteins were started to be ablated from E13.5 and were completely knocked out after E15.5 (Figures 1A and 1B).

We then checked the cortical neurogenesis of *Ythdf1* and *Ythdf2* scKO mice. The numbers of either Pax6-labeled radial glia cells or Tbr2-marked intermediate progenitors showed no difference between the scKO and its corresponding control at P0 (Figures 2A–2E). The scKO cortex also exhibited no difference in thickness of cortical layers identified by Tbr1/Ctip2 co-staining at P5 (Figures 2F–2H). Together, these results indicate that knockout of *Ythdf1* or *Ythdf2* individually does not affect cortical neurogenesis, and thus cannot recapitulate the phenotypes of *Mettl14* cKO.

Double knockout of *Ythdf1* and *Ythdf2* causes cortical neurogenesis defects

Because individual deletion of *Ythdf1* or *Ythdf2* could not affect cortical neurogenesis as *Mettl14* cKO, we further generated the double conditional knockout (dcKO) of *Ythdf1* and *Ythdf2* (*Nesin-cre*$^{+/-}$, *Ythdf1*$^{fl/fl}$, *Ythdf2*$^{fl/fl}$, *Y1Y2* dcKO) to ablate *Ythdf1* and *Ythdf2* simultaneously and examine the effect of loss-of-function of both readers on cortical neurogenesis. We first verified the efficient knockout of both YTHDF1 and YTHDF2 in the dcKO mice with anti-YTHDF1 and YTHDF2 immunostaining (Figures 3A and 3B).

Next, we examined the radial glia cells and the intermediate progenitors in the dcKO cortex. Significant increases in the numbers of Pax6$^+$ radial glia cells and Tbr2$^+$ intermediate progenitors were observed in

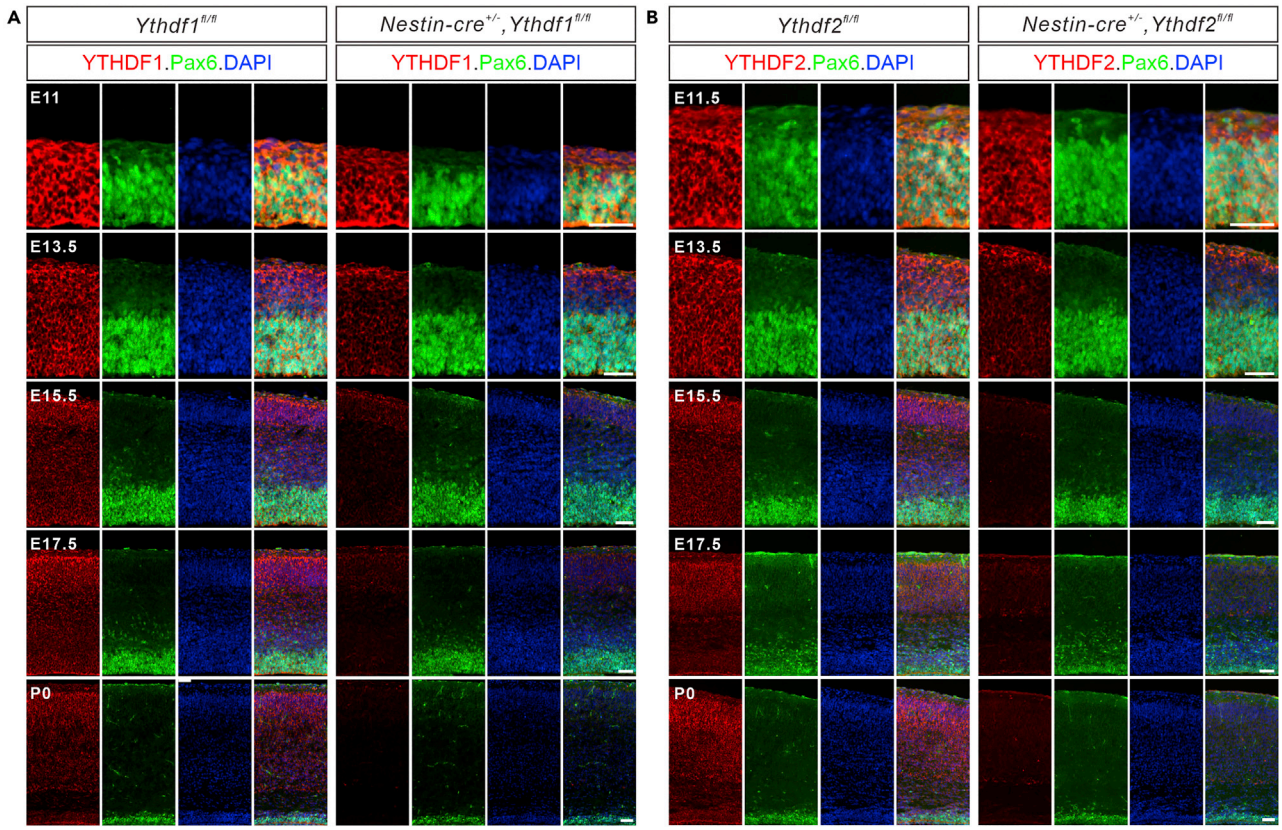

Figure 1. YTHDF1 and YTHDF2 are highly expressed and efficiently ablated in the *Ythdf1* and *Ythdf2* cKO cortices

(A and B) Representative images showing immunostaining of YTHDF1 (A) or YTHDF2 (B) and Pax6 in coronal sections of *Ythdf1* (A) or *Ythdf2* (B) scKO and littermate controls at E11 or E11.5, E13.5, E15.5, E17.5, and P0. As shown, YTHDF1 and YTHDF2 are highly expressed in the radial glia cells from E11. Partial knockout of YTHDF1 and YTHDF2 could be observed from E13.5, and complete knockout was achieved from E15.5. Scale bars, 50 μm.

the dcKO cortex at P0 (Figures 3C and 3D). To determine whether cell cycle exit of radial glia cells was affected in the dcKO cortex, we performed co-staining of BrdU and Ki67 in E17.5 cortical sections collected after 24 h of BrdU injection (Figure 3E). There is a significant decrease in the percentage of $Ki67^{-}BrdU^{+}$/$BrdU^{+}$, suggesting a delay in cell cycle exit of radial glial cells in the dcKO cortex (Figure 3F). Then we assessed the cortical layer thickness. Although the thickness of layers WM-VZ and earlier born layer VI did not change, the thickness of layer V and later born layers I-IV significantly decreased (Figure 3G).

Together, our findings demonstrate that the dcKO of *Ythdf1* and *Ythdf2* causes prolonged cell cycle and maintenance of radial glia cells, and decreased generation of neurons in the cortex, recapitulating the phenotypes of *Mettl14* cKO. These results suggest that YTHDF1 and YTHDF2 have redundant functions in mediating m^6A regulation of cortical neurogenesis.

We continued to check the cortical neurogenesis of the *Ythdf3* cKO mice using *Nestin-cre*. We found no difference in the numbers of Pax6-labeled radial glia cells or Tbr2-marked intermediate progenitors between *Ythdf3* cKO and littermate control at P0 (Figures S2A and S2B). The *Ythdf3* cKO cortex also showed no difference in thickness of cortical layers identified by Tbr1/Ctip2 co-staining at P5 (Figure S2C). Together, these results suggest that *Ythdf3* cKO does not affect cortical neurogenesis.

Mettl14 ablation in retina protracts retinal neurogenesis and leads to reduced generation of late-born neurons

Next we tested whether and how m^6A modification regulates neurogenesis in other brain regions. To explore whether m^6A modification mediates retinal neurogenesis, we first checked the m^6A modification level in the embryonic retina. Abundant m^6A modification was detected in the retinal progenitors and

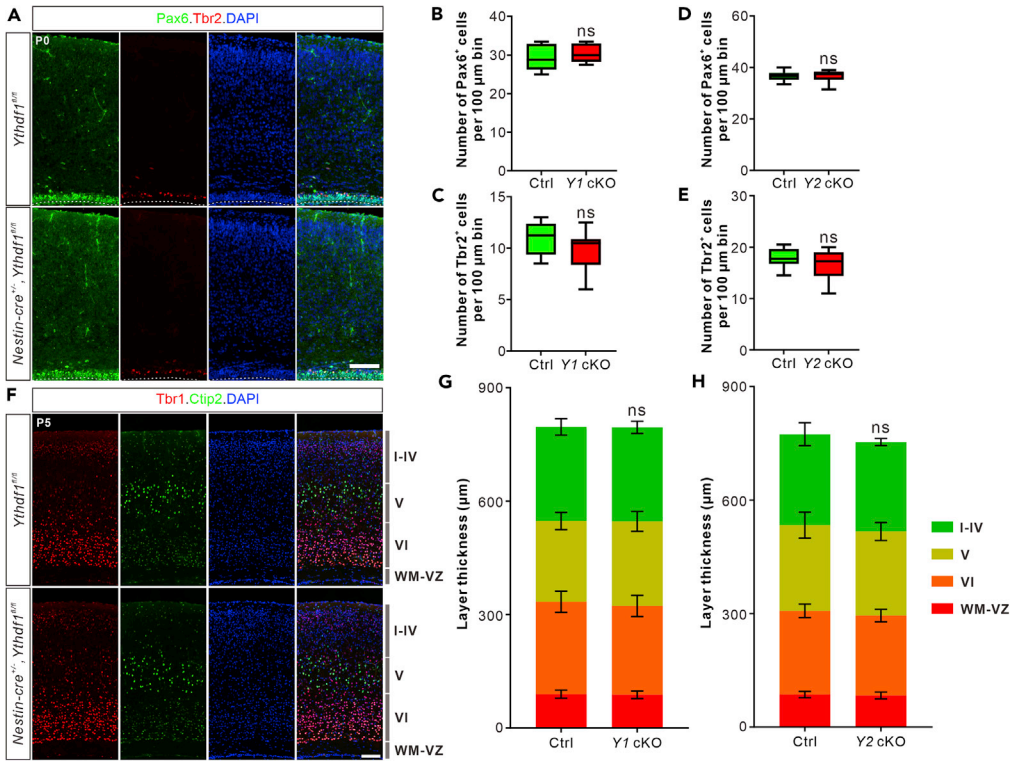

Figure 2. *Ythdf1* or *Ythdf2* conditional knockout mice show no defect in cortical neurogenesis

(A) Representative images of coronal sections of P0 *Ythdf1*$^{fl/fl}$ and *Nestin-cre*$^{+/-}$,*Ythdf1*$^{fl/fl}$ cortices immunostained with Pax6 and Tbr2 to label radial glia cells and intermediate progenitors, respectively.

(B–E) Quantification of Pax6^{+} radial glial cells (B and D) and Tbr2^{+} intermediated progenitors (C and E). Numbers of corresponding cells per 100 μm bin of cortical coronal sections were quantified and showed no difference between the *Ythdf1* scKO (*Y1* cKO, n = 8 sections) or *Ythdf2* scKO (*Y2* cKO, n = 8 sections) and their corresponding littermate controls (Ctrl, n = 8 sections) at P0. Data are represented as box and whisker plots: p = 0.43 for B, p = 0.21 for C; p = 0.96 for D, p = 0.29 for E; ns, not significant; by unpaired Student's *t* test.

(F) Representative images of coronal sections of P5 *Ythdf1*$^{fl/fl}$ and *Nestin-cre*$^{+/-}$,*Ythdf1*$^{fl/fl}$ cortices immunostained with Tbr1 and Ctip2 to distinguish different cortical layers.

(G and H) Measurement and quantification of cortical layer thickness. The thickness of layers WM-VZ, VI, V, I–IV, and whole cortex was measured and showed no difference between the scKO (n = 30 sections for *Y1* cKO in G, n = 21 sections for *Y2* cKO in (H)) and littermate controls (n = 30 sections for Ctrl in G, n = 21 sections for Ctrl in H) at P5. Data are represented as accumulative histogram: in G, p = 0.56 for layers WM-VZ, p = 0.20 for layer VI, p = 0.13 for layer V, p = 0.96 for layers I–IV, p = 0.94 for whole cortex; in H, p = 0.38 for layers WM-VZ, p = 0.067 for layer VI, p = 0.66 for layer V, p = 0.60 for layers I–IV, p = 0.069 for whole cortex; ns, not significant; by unpaired Student's *t* test. Scale bars, 100 μm.

retinal ganglion cells (RGCs) at E14.5 (Figure S3A). Then, we generated *Mettl14* cKO mouse by crossing *Mettl14* $^{fl/fl}$ with *Six3-cre* mouse which has been widely used in the studies of retinal neurogenesis (Furuta et al., 2000; Krishnaswamy et al., 2015; Luo et al., 2012; Sapkota et al., 2014). METTL14 immunostaining in E12.5, E15.5, and P0 retinal vertical sections revealed that METTL14 expression was high in the developing retinas (control retinas in Figures 4A–4C), and was efficiently ablated in the *Mettl14* cKO retina (Figures 4A–4C). Furthermore, *Mettl14* cKO retina exhibited significantly lower m^{6}A levels compared with littermate control (Figure S3A), suggesting that m^{6}A modification is largely restricted in retina after *Mettl14* deletion.

To check the retinal neurogenesis in *Mettl14* cKO, we examined the major retinal cell and neuron types by immunostaining of vertical retinal sections with different markers: Ki67, a proliferation marker; Brn3a, a marker for retinal ganglion cells (Brodie-Kommit et al., 2021); AP2α, a marker for amacrine cells (Hicks et al., 2018); PKCα, a marker for rod bipolar cells (Lu et al., 2013). During mouse retinal neurogenesis, retinal progenitors are largely depleted by P6 (control retina in Figure 4D). However, a substantial number of Ki67^{+} cells were still present in the *Mettl14* cKO retina (Figures 4D and 4E). Retinal ganglion cells, as the early born

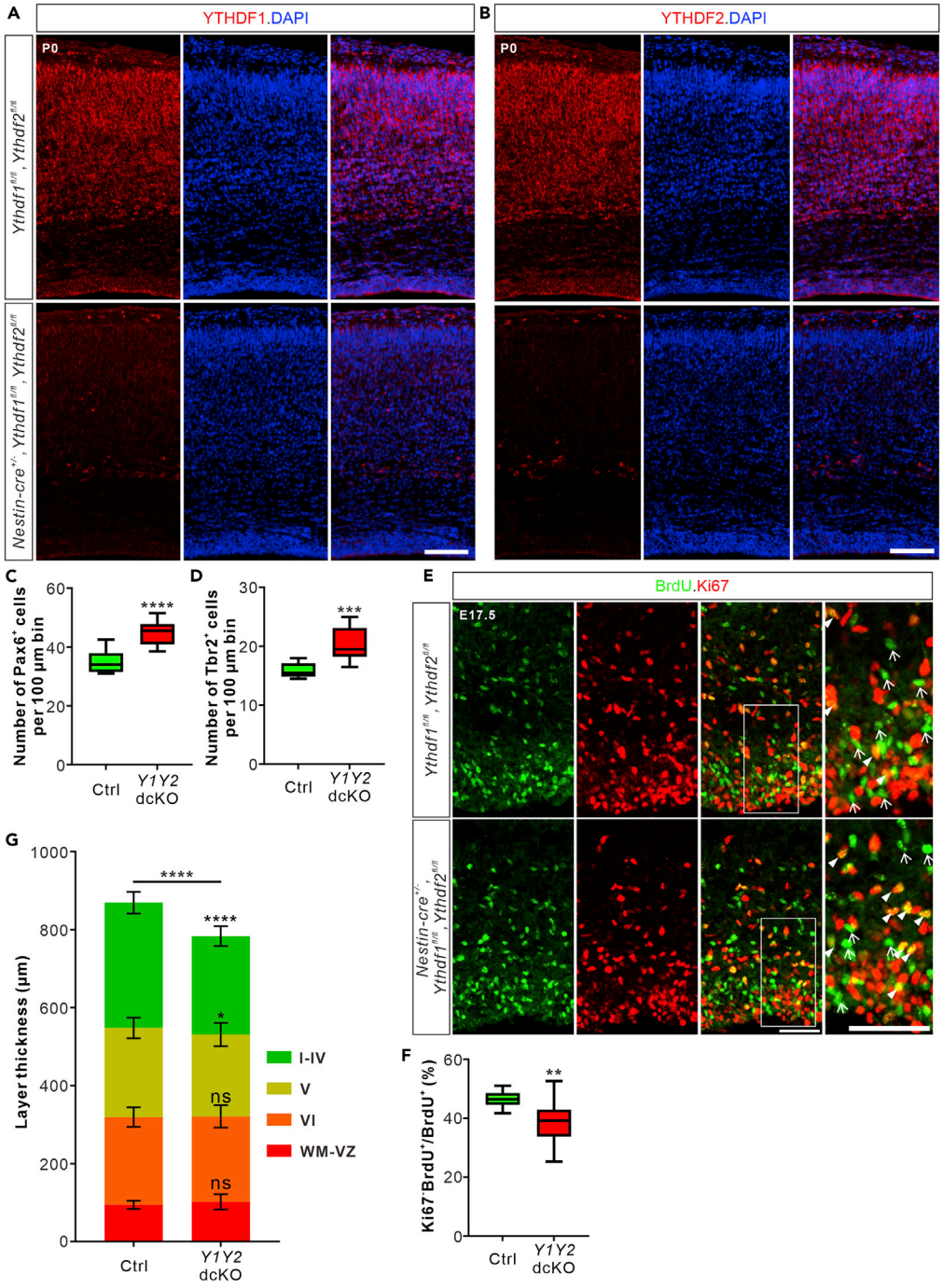

Figure 3. Simultaneous knockout of *Ythdf1* and *Ythdf2* causes cortical neurogenesis defects

(A and B) Representative images of coronal sections of *Ythdf1*$^{fl/fl}$,*Ythdf2*$^{fl/fl}$ (Ctrl) and *Nestin-cre*$^{+/-}$,*Ythdf1*$^{fl/fl}$,*Ythdf2*$^{fl/fl}$ (*Y1Y2* dcKO) cortices immunostained with YTHDF1 (A) and YTHDF2 (B) at P0. YTHDF1 and YTHDF2 were knocked out efficiently in the dcKO mice.

(C and D) Quantification of Pax6^{+} radial glial cells (C) and Tbr2^{+} intermediated progenitors (D). Numbers of corresponding cells per 100 μm bin of cortical coronal sections were quantified and showed increases in the dcKO (n = 10 sections) compared with the littermate control (Ctrl, n = 10 sections) at P0. Data are represented as box and whisker plots: ****p = 3.27 × 10^{-5} for C, ***p = 0.00018 for D; by unpaired Student's *t* test.

Figure 3. *Continued*

(E) Representative images of Ki67 and BrdU co-labeling of coronal cortical sections at E17.5. Pregnant mice were injected with BrdU 24 h before collecting embryos. The arrowheads indicate the $Ki67^{+}BrdU^{+}$ cells and the arrows point to the $Ki67^{-}BrdU^{+}$ cells.

(F) Quantification of results in E. The percentage of $Ki67^{-}BrdU^{+}/BrdU^{+}$, representing the ratio of cells exiting cell cycle, decreased in the dcKO (n = 10 sections) compared with littermate controls (n = 10 sections). Data are represented as box and whisker plots: **p = 0.0091, by unpaired Student's *t* test.

(G) Measurement and quantification of the thickness of cortical layers at P5. The thickness of layers WM-VZ and layer VI showed no difference between the dcKO and control mice. The thickness of layer V, layers I-IV, and whole cortex decreased in the dcKO cortex (n = 27 sections) compared with littermate controls (n = 23 sections). Data are represented as an accumulative histogram: p = 0.10 for layers WM-VZ, p = 0.44 for layer VI, *p = 0.025 for layer V, ****p = 9.10E-12 for layers I–IV, ****p = 2.98E-05 for whole cortex; ns, not signification; by unpaired Student's t-test. Scale bars, 100 μm (A,B) and 50 μm (E).

neuron type in the retina, are normally located at the basal ganglion cell layer (GCL) after being differentiated from retinal progenitors at E15.5 and P0 (control retina in Figures 4B and 4C) (Cepko, 2014). However, in the *Mettl14* cKO retina, some of retinal ganglion cells were dislocated at the apical retina revealed by Brn3a immunostaining (Figures 4B and 4C). In addition, the distribution of $Brn3a^{+}$ retinal ganglion cells in the basal retina was also disturbed in the *Mettl14* cKO retina at P6 (Figure 4F). $AP2\alpha^{+}$ amacrine cells dramatically decreased in the *Mettl14* cKO retina compared with control retina at P6 (Figures 4G and 4H). Generation and patterning of retinal bipolar cells were severely impaired (Figures 4I and 4J). Besides the decreased numbers of retinal neurons, the structure of the *Mettl14* cKO retinas was deformed and the retinal layers were disorganized compared with control retinas (Figures 4C, 4D, 4F, 4G, and 4I). All together, these results indicate that *Mettl14* cKO in retina leads to extended retinal neurogenesis, decreased generation of late-born neurons, and deformed retinal patterning.

Single or double conditional knockout of *Ythdf1* and *Ythdf2* in retina does not affect retinal neurogenesis

Next, we wanted to identify which readers mediate m^6A functions in retinal neurogenesis. We first focused on YTHDF1 and YTHDF2 which are expressed in the developing retinas (Niu et al., 2022) (control retinas in Figure S4A). We generated *Ythdf1* and *Ythdf2* single conditional knockouts in retina using *Six3-cre*: *Six3-cre*$^{+/-}$, *Ythdf1*$^{fl/fl}$ (*Ythdf1* scKO) and *Six3-cre*$^{+/-}$,*Ythdf2*$^{fl/fl}$ (*Ythdf2* scKO). We have previously shown that although retinal ganglion cell dendrite branching increases, retinal neurogenesis is not affected in the *Ythdf2* scKO (Niu et al., 2022).

We continued to check the *Ythdf1* scKO. Immunostaining of YTHDF1 confirmed that YTHDF1 was efficiently knocked out in the *Ythdf1* scKO retinas (Figure S4A). Immunostaining of Brn3a, AP2α and PKCα on the retinal vertical sections showed that generation of retinal ganglion cells, amacrine cells, or bipolar cells was not affected in the *Ythdf1* scKO retinas at P6 and P15 (Figures S4B–S4F). These results and our previous findings (Niu et al., 2022) together suggest that knockout of *Ythdf1* or *Ythdf2* alone does not affect retinal neurogenesis.

Because YTHDF1 and YTHDF2 function redundantly to mediate m^6A modification in regulating cortical neurogenesis (Figures 2 and 3), we wondered if there is a similar mechanism in the retinal neurogenesis. So we generated double conditional knockout of *Ythdf1* and *Ythdf2* (*Y1Y2* dcKO) in retina (*Six3-cre*$^{+/-}$, *Ythdf1*$^{fl/fl}$, and *Ythdf2*$^{fl/fl}$) to ablate *Ythdf1* and *Ythdf2* in the retina simultaneously (Figures 5A and 5B). However, we surprisingly found that numbers of retinal ganglion cells, amacrine cells, or bipolar cells were not changed in the *Y1Y2* dcKO retinas (Figures 5C–5E). Together, these data suggest that single or double conditional knockout of *Ythdf1* and *Ythdf2* in retina has no effect on retinal neurogenesis.

Triple knockout of *Ythdf1*, *Ythdf2*, and *Ythdf3* in retina extends retinal progenitor proliferation and decreases generation of late-born retinal neurons

Because single or double conditional knockout of *Ythdf1* and *Ythdf2* cannot recapitulate the phenotype of *Mettl14* cKO in retina, we continued to check another m^6A reader, YTHDF3. We first checked expression of *Ythdf3* in retina using *in situ* hybridization (ISH), which detected signals in the developing retina (control retina in Figure S5A). Then we generated *Ythdf3* cKO mice (Figure S5B), and Six3-Cre induced efficient knockout of *Ythdf3* in retina (*Six3-cre*$^{+/-}$, *Ythdf3*$^{fl/fl}$, and *Ythdf3* cKO) (Figure S5A). We further checked

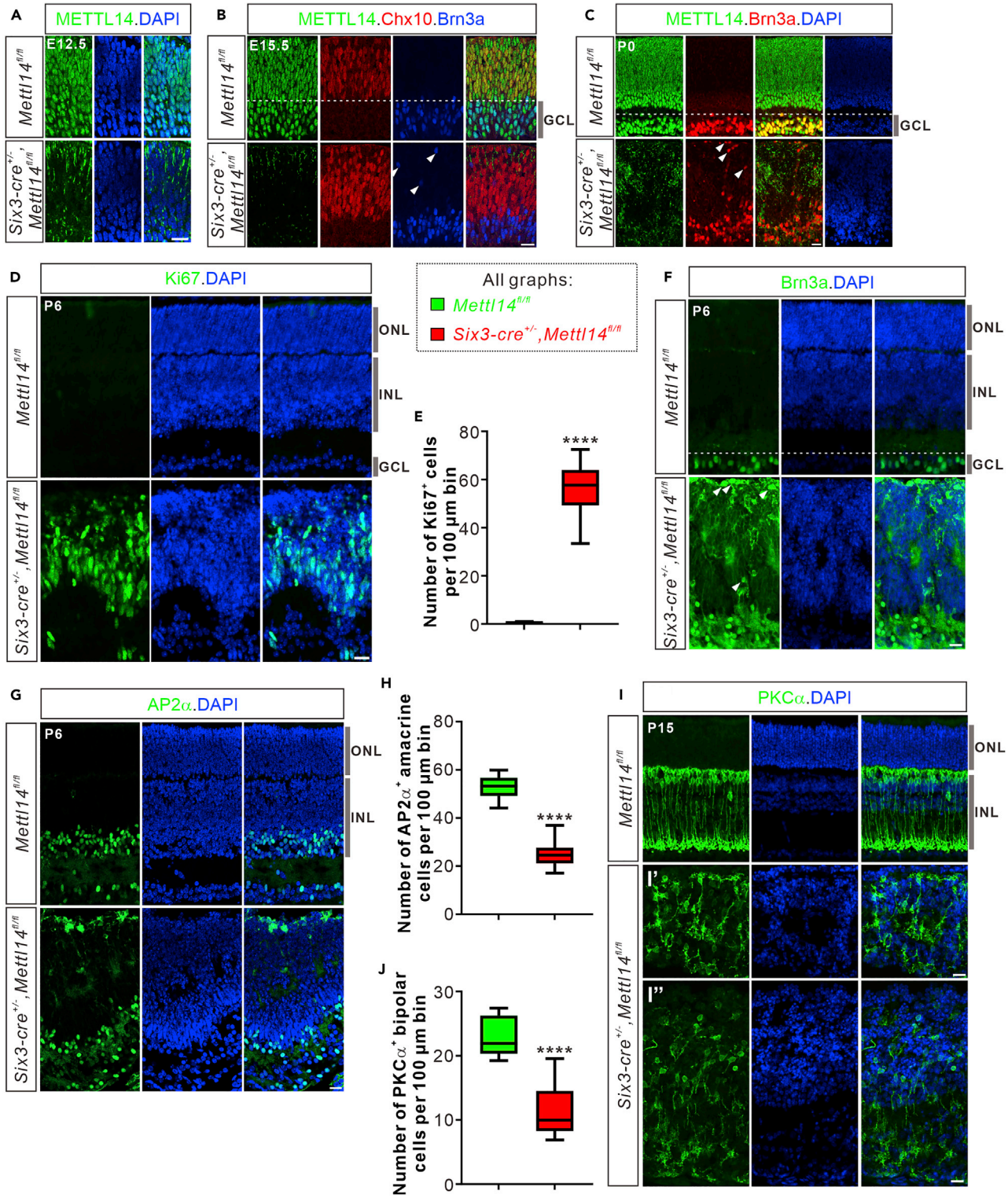

Figure 4. *Mettl14* ablation in retina protracts retinal neurogenesis and leads to reduced generation of late-born neurons

(A–C) Representative images of vertical sections from *Mettl14* cKO (*Six3-cre*$^{+/-}$,*Mettl14*$^{fl/fl}$) and control (*Mettl14*$^{fl/fl}$) retinas immunostained with METTL14 at E12.5 (A), E15.5 (B), and P0 (C). METTL14 expression is high in the control retinas and is efficiently ablated in the *Mettl14* cKO retinas. The residual bright signals in the cKO sections are non-specific immunofluorescence signals with this METTL14 Ab. Chx10 and Brn3a are the markers for retinal progenitor cells and retinal ganglion cells, respectively. The arrowheads indicate the misplaced Brn3a^{+} RGCs (B and C). GCL, ganglion cell layer.

Figure 4. *Continued*

(D) Representative images of P6 *Mettl14* cKO and control retinas immunostained with the proliferation cell marker Ki67. ONL, outer nuclear layer; INL, inner nuclear layer.

(E) Quantification of Ki67$^+$ retinal progenitor cell numbers in (D). The cell numbers per 100 μm bin of retinal vertical sections were quantified. The retinal progenitors were abnormally maintained in the *Mettl14* cKO retina at P6. Data are represented as box and whisker plots: n = 12 sections for *Mettl14* cKO and control, respectively; ****p = 7.00E-15; by unpaired Student's *t* test.

(F) Representative images of P6 *Mettl14* cKO and control retinas immunostained with Brn3a. Misplaced Brn3a$^+$ retinal ganglion cells (arrowheads) were found in the *Mettl14* cKO retina.

(G) Representative images of P6 *Mettl14* cKO and control retinas immunostained with AP2α. AP2α marks the amacrine cells.

(H) Quantification of AP2α$^+$ amacrine cell numbers in G. Numbers of AP2α$^+$ amacrine cells per 100 μm bin of retinal vertical sections were quantified and decreased in the *Mettl14* cKO (n = 12 sections) compared with littermate controls (n = 12 sections) at P6. Data are represented as box and whisker plots: ****p = 1.27E-11; by unpaired Student's *t* test.

(I) Representative images of the vertical sections immunostained with the bipolar cell marker PKCα from *Mettl14* cKO and control retinas at P15. Please note that the cKO retinas are severely deformed at P15, and their thicknesses are not even with some areas becoming much thinner (I') and others thicker (I'') compared with control retinas. The organization of bipolar cells was totally messed up.

(J) Quantification of PKCα$^+$ bipolar cell numbers in I. Numbers of PKCα$^+$ bipolar cells per 100 μm bin of retinal vertical sections were quantified and decreased in the *Mettl14* cKO (n = 17 sections) compared with littermate controls (n = 15 sections) at P15. Data are represented as box and whisker plots: ****p = 6.96E-11; by unpaired Student's *t* test. Scale bars, 20 μm (A–C, D, F, G, and I).

retinal neurogenesis of *Ythdf3* cKO in retina. As shown in Figures S5C–S5E, generation of retinal ganglion cells, amacrine cells, or bipolar cells was not affected in the *Ythdf3* cKO retinas.

We continued to generate triple conditional knockout of *Ythdf1*, *Ythdf2*, and *Ythdf3* (*Y1Y2Y3* tcKO) in retina (*Six3-cre*$^{+/-}$, *Ythdf1*$^{fl/fl}$, *Ythdf2*$^{fl/fl}$, and *Ythdf3*$^{fl/fl}$) which exhibited efficient knockout of YTHDF1 and YTHDF2 by immunostaining (Figures 6A and 6B) and *Ythdf3* by ISH (Figure 6C) at P0. Then we checked retinal neurogenesis in the *Y1Y2Y3* tcKO mice. Ki67$^+$ retinal progenitors were abnormally maintained in the tcKO retinas at P6 (Figures 6D and 6E). Retinal ganglion cells showed disordered location in the tcKO retinas at P6 (Figure 6F). Numbers of AP2α$^+$ amacrine cells at P6 and PKCα$^+$ bipolar cells at P15 were decreased in the tcKO retinas (Figures 6G–6J). In addition, retinal layers were also disorganized and neurons were misplaced in the tcKO retinas (Figures 6D, 6F, 6G, and 6I). These results demonstrate that *Y1Y2Y3* tcKO leads to prolonged retinal neurogenesis and impaired generation of late-born retinal neurons.

All these data suggest that YTHDF1, YTHDF2 and YTHDF3 function redundantly to mediate m^{6}A modification in retinal neurogenesis, and simultaneous knockout of *Ythdf1*, *Ythdf2*, and *Ythdf3* can recapitulate the retinal neurogenesis defects caused by *Mettl14* conditional knockout in retina.

We next continued to test whether other YTHDFs were upregulated to compensate the single *Ythdf* cKO. By RT-qPCR analysis, the expression levels of *Ythdf2* and *Ythdf3* mRNAs were not changed after *Ythdf1* knockout (Figures S6A and S6B). In the *Ythdf2* cKO retina, the expression levels of *Ythdf1* and *Ythdf3* mRNAs were also not affected (Figures S6D and S6E). Similarly, the expression levels of *Ythdf1* and *Ythdf2* mRNAs were not changed in the *Ythdf3* cKO retina (Figures S6G and S6H). Next, we also checked the protein levels of YTHDF1 and YTHDF2 in the *Ythdf* scKO retinas by IF. Similarly as its mRNA level, YTHDF2 protein expression also exhibited no difference between *Ythdf1* scKO and Ctrl (Figure S6C). Similarly, YTHDF1 protein expression was also not changed in *Ythdf2* scKO (Figure S6F). In addition, YTHDF1 and YTHDF2 protein levels were not affected in *Ythdf3* scKO (Figures S6I and S6J). These results suggest that single cKO of each *Ythdfs* does not affect mRNA or protein levels of other YTHDFs.

YTHDF1 and YTHDF2 share a large pool of target mRNAs related to neurogenesis in mouse cortex and retina

To further explore the mechanisms by which the m^{6}A readers mediate m^{6}A modification in regulating neurogenesis, we continued to identify the target mRNAs of YTHDFs. We performed anti-YTHDF1 and anti-YTHDF2 RNA immunoprecipitation followed by RNA sequencing of the elutes (RIP-seq) in the developing cortex and retina. From the embryonic cortex, we identified 986 and 1860 mRNAs by anti-YTHDF1 and anti-YTHDF2 RIP-seq, respectively (Figure 7A and Table S1). 596 mRNAs were identified to be common targets of YTHDF1 and YTHDF2 (Figure 7A and Table S1). Gene Ontology (GO) analysis of those target mRNAs revealed enrichment of genes related to regulation of nervous system development, regulation of neuron differentiation, regulation of neurogenesis et al. (Figures 7B, S7A, and S7B), which is consistent with the redundant functions of YTHDF1 and YTHDF2 in mediating m^{6}A regulation of cortical neurogenesis.

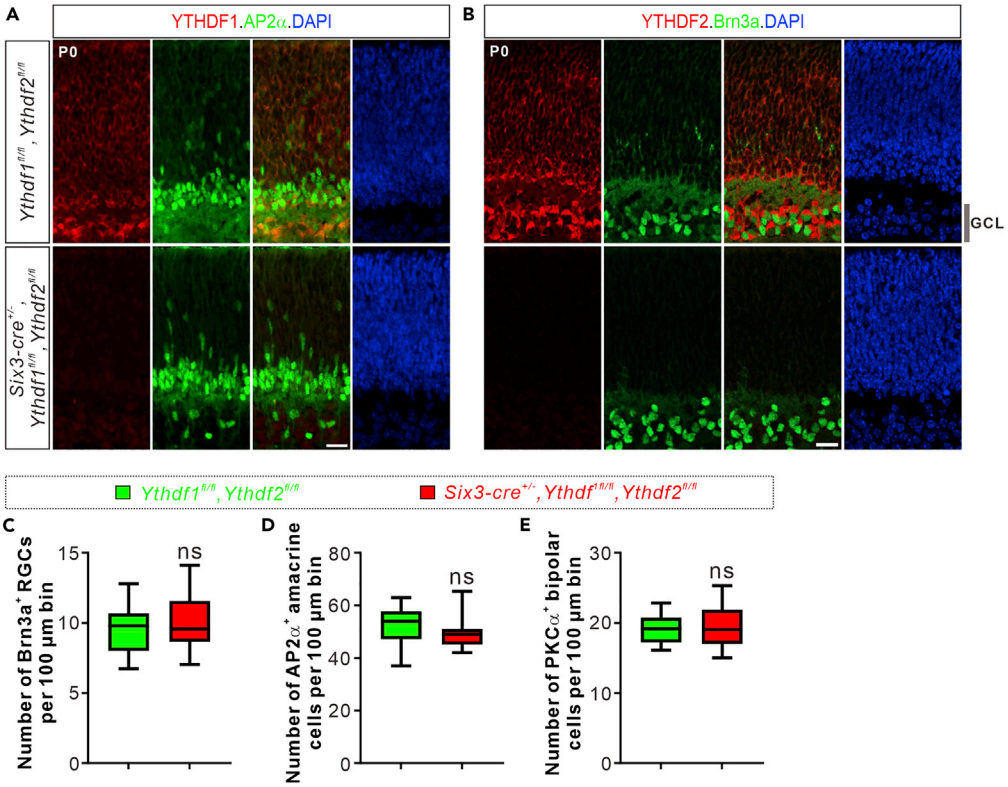

Figure 5. Double conditional knockout of *Ythdf1* and *Ythdf2* in retina does not disturb retinal neurogenesis

(A and B) Representative images of the retinal vertical sections co-stained with YTHDF1 and AP2α (A), YTHDF2 and Brn3a (B) from *Ythdf1*$^{fl/fl}$,*Ythdf2*$^{fl/fl}$ and *Six3-cre*$^{+/-}$,*Ythdf1*$^{fl/fl}$,*Ythdf2*$^{fl/fl}$ (*Y1Y2* dcKO) retinas at P0.

(C–E) Quantification of numbers of Brn3a$^+$ retinal ganglion cells (C), AP2α$^+$ amacrine cells (D), and PKCα$^+$ bipolar cells (E) in the *Y1Y2* dcKO and control retinas. Numbers of corresponding cell types per 100 μm bin of retinal vertical sections were quantified and showed no difference between the dcKO and control retinas. All quantification data are represented as box and whisker plots: in (C), n = 16 sections for dcKO, n = 16 sections for control, p = 0.67; in D, n = 16 sections for dcKO, n = 16 sections for control, p = 0.18; in E, n = 22 sections for dcKO, n = 12 sections for control, p = 0.94; ns, not signification; by unpaired Student's t test. Scale bars, 20 μm (A and B).

We have previously shown that anti-YTHDF2 RIP-seq in mouse retina identified 1638 mRNAs (Niu et al., 2022). We also carried out anti-YTHDF1 RIP-seq in mouse retina and identified 2969 mRNAs (Figure 7C and Table S2). By comparing these two groups of mRNAs, we found that 1029 mRNAs are common targets of YTHDF1 and YTHDF2 in retina (Figure 7C and Table S2). Similarly as cortex, GO analysis of those target mRNAs revealed enrichment of genes related to neuron differentiation, nervous system development, neurogenesis et al. (Figures 7D and S7C).

Together, those results demonstrated that YTHDF1 and YTHDF2 share a large pool of target mRNAs related to neurogenesis in mouse cortex and retina, supporting their redundant functions in mediating m^{6}A regulation of cortical and retinal neurogenesis.

Next we wanted to narrow down and identify the driver targets. By overlapping the common cortical targets of YTHDF1 and YTHDF2 with the m^{6}A-enriched cortical transcripts from Yoon et al. (2017), 146 mRNAs were identified as m^{6}A-enriched common targets of YTHDF1 and YTHDF2 (Table S3).

We further overlapped the common cortical target mRNAs of YTHDF1/2 with the differentially expressed genes in cortical neural progenitor cells (NPCs) of *Mettl14* cKO mouse from Yoon et al. (2017). 107 mRNAs were identified, and 95 of them were upregulated after *Mettl14* deletion (Table S4). We further focused on *Arid1b*, *Atoh8*, and *Sema4c*. ARID1B, a subunit of the BAF chromatin remodeling complex, was linked to autism spectrum disorder (ASD) and intellectual disability (Moffat et al., 2019). Recently, ARID1B was

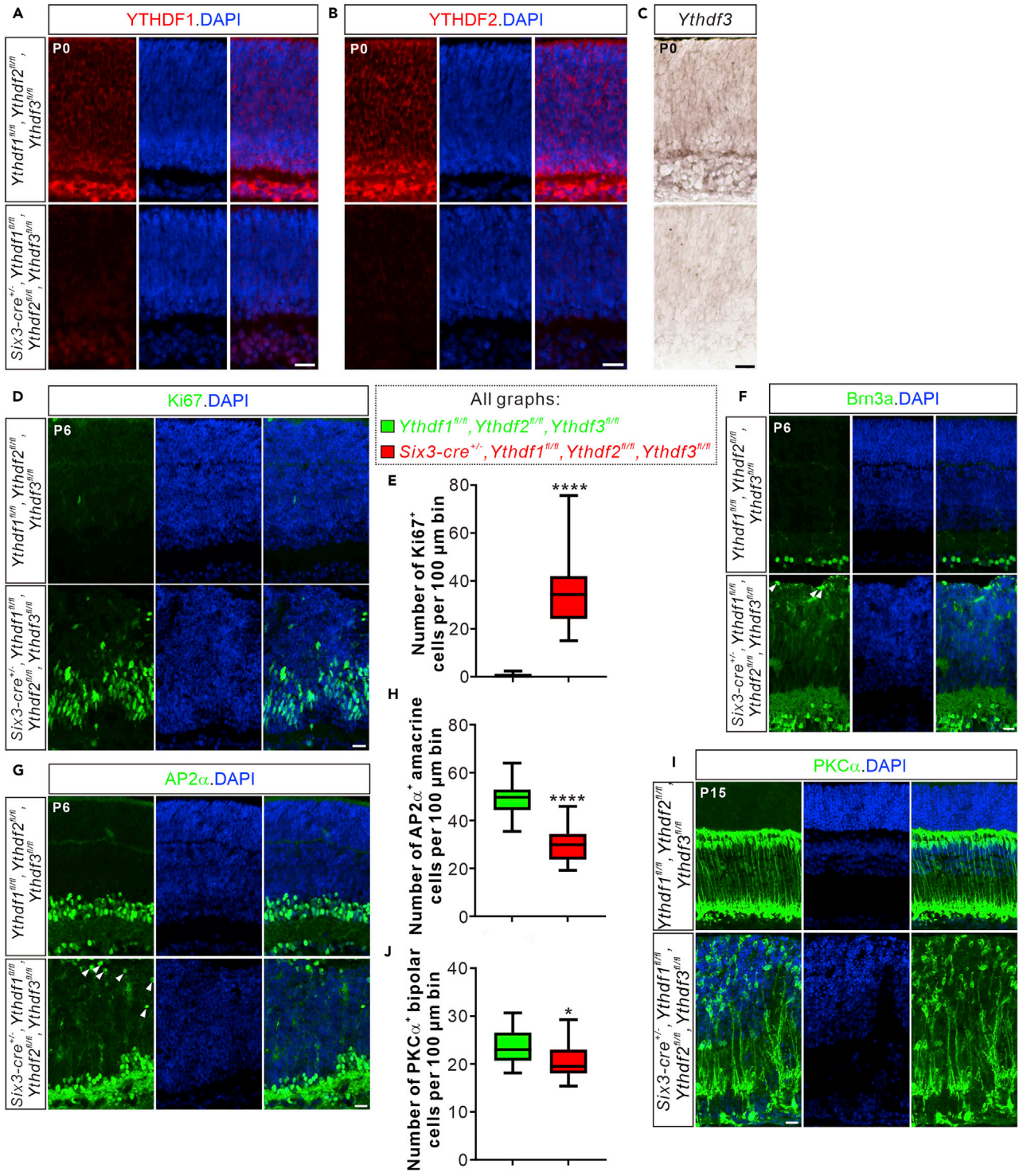

Figure 6. Triple knockout of *Ythdf1*, *Ythdf2*, and *Ythdf3* in retina extends retinal progenitor proliferation and decreases generation of late-born retinal neurons

(A and B) Representative images of the vertical sections immunostained with YTHDF1 and YTHDF2 showing efficient knockout of *Ythdf1* and *Ythdf2* in the*Y1Y2Y3* triple cKO retinas at P0.

(C) Representative ISH images of the vertical sections showing efficient ablation of *Ythdf3* in the *Y1Y2Y3* triple cKO retinas at P0.

Figure 6. *Continued*

(D) Representative images of the retinal vertical sections immunostained with the retinal progenitor marker Ki67. While Ki67$^+$ cells were absent from the control (*Ythdf1*$^{fl/fl}$, *Ythdf2*$^{fl/fl}$, and *Ythdf3*$^{fl/fl}$) retinas at P6, there were still a lot of Ki67$^+$ cells in the *Y1Y2Y3* tcKO (*Six3-cre*$^{+/-}$, *Ythdf1*$^{fl/fl}$, *Ythdf2*$^{fl/fl}$, and *Ythdf3*$^{fl/fl}$) retinas at P6.

(E) Quantification of numbers of Ki67$^+$ retinal progenitors in (A). Numbers of Ki67$^+$ retinal progenitors per 100 μm bin of retinal vertical sections were quantified and abnormally maintained in the *Y1Y2Y3* triple cKO (n = 20 sections) compared with littermate controls (n = 13 sections). Data are represented as box and whisker plots: ****p = 1.67E-09, by unpaired Student's *t* test.

(F) Representative images of the retinal vertical sections immunostained with Brn3a, the retinal ganglion cell marker. The location and organization of Brn3a$^+$ retinal ganglion cells were disturbed in the *Y1Y2Y3* tcKO retinas at P6. Arrowheads indicate the misplaced Brn3a$^+$ retinal ganglion cells.

(G) Representative images of the vertical sections with amacrine cells marked by AP2α in the *Y1Y2Y3* tcKO and control retinas at P6. AP2α$^+$ amacrine cells were decreased and disorganized in the *Y1Y2Y3* tcKO retinas. Arrowheads indicate the misplaced AP2α$^+$ amacrine cells.

(H) Quantification of numbers of AP2α$^+$ amacrine cells in (D). Numbers of AP2α$^+$ amacrine cells per 100 μm bin of retinal vertical sections were quantified and showed decreases in the *Y1Y2Y3* tcKO (n = 20 sections) compared with littermate controls (n = 14 sections). Data are represented as box and whisker plots: ****p = 8.01E-09, by unpaired Student's *t* test.

(I) Representative images of the vertical sections with bipolar cells labeled by PKCα in the *Y1Y2Y3* tcKO and control retinas at P15. The organization of PKCα$^+$ bipolar cells was severely disturbed.

(J) Quantification of numbers of PKCα$^+$ bipolar cells in (F). Numbers of PKCα$^+$ bipolar cells per 100 μm bin of retinal vertical sections were quantified and showed decreases in the *Y1Y2Y3* tcKO (n = 20 sections) compared with littermate controls (n = 24 sections). Data are represented as box and whisker plots: *p = 0.011, by unpaired Student's *t* test. Scale bars, 20 μm (A–C, D, F, G, and I).

reported to regulate the proliferation and differentiation of NPCs (Moffat et al., 2021; Yang et al., 2021). Atoh8, also known as Math6, was accumulated in the developing brain and modulated neuron differentiation (Li et al., 2019; Wang et al., 2015a). Sema4c is a transmembrane protein which could interacts with PSD95, was expressed abundantly in NPCs and regulated adult neurogenesis induced by cerebral ischemia (Wu et al., 2009). We next performed RT-qPCR to check the expression levels of these targets in E14 *Y1Y2* dcKO mouse. *Arid1b*, *Atoh8*, and *Sema4c* mRNA levels were dramatically increased in the *Y1Y2* dcKO cortex compared with controls (Figures S7D–S7F), suggesting that they might be the driver targets of YTHDF1 and YTHDF2 to mediate m^{6}A regulation of cortical neurogenesis.

DISCUSSION

In this study, we revealed the redundant functions of the m^{6}A readers YTHDFs to mediate m^{6}A modification in regulating cortical and retinal neurogenesis.

m^{6}A modification has been found to control mammalian cortical neurogenesis (Wang et al., 2018; Yoon et al., 2017). One study found that conditional knockout of the writer METTL14 caused prolonged cell cycle and remnant of radial glia cells (Yoon et al., 2017). Another study reported that *Mettl14* conditional knockout led to decreased proliferation and premature differentiation (Wang et al., 2018). This obvious inconsistency calls for further exploration and clarification of the functions of m^{6}A modification in cortical neurogenesis. Here we found that *Mettl14* deletion causes abnormal maintenance of radial glia cells in the postnatal stages, delays cortical neurogenesis, and reduces production of neurons, supporting the findings by Yoon et al. (2017).

We further showed that m^{6}A regulation of neurogenesis is working similarly in other brain regions. Deletion of *Mettl14* in retina extends maintenance of proliferating retinal progenitors, decreases production of late-born neurons, and impairs organization of retinal layers. These findings support a general role of m^{6}A modification in regulating neurogenesis.

The YTHDF family proteins, YTHDF1, YTHDF2, and YTHDF3 are the major cytosolic m^{6}A reader proteins to mediate m^{6}A functions by regulating degradation and translation of target mRNAs (Kontur et al., 2020; Lasman et al., 2020; Shi et al., 2017; Wang et al., 2014, 2015b; Zaccara and Jaffrey, 2020). However, which m^{6}A readers and how they mediate m^{6}A modification in neurogenesis are still unknown. Here we found that single conditional knockout of *Ythdf1*, *Ythdf2* or *Ythdf3* has no effect on cortical neurogenesis. Double deletion of *Ythdf1* and *Ythdf2* leads to protracted cortical neurogenesis, delayed cell-cycle exit, and reduced late-born neurons, which is consistent with the neurogenesis phenotypes of *Mettl14* conditional knockout in cortex. In retina, single or double knockout of *Ythdf1*, *Ythdf2* does not disturb retinal neurogenesis. Triple conditional knockout of *Ythdf1*, *Ythdf2*, and *Ythdf3* exhibits extended neurogenesis, disordered lamination, and decreased late-born neurons, resembling the neurogenesis phenotypes of *Mettl14* conditional knockout in retina. Identification of common target mRNAs recognized by both YTHDF1 and YTHDF2 further supports the redundant functions of YTHDFs in mediating cortical and retinal neurogenesis.

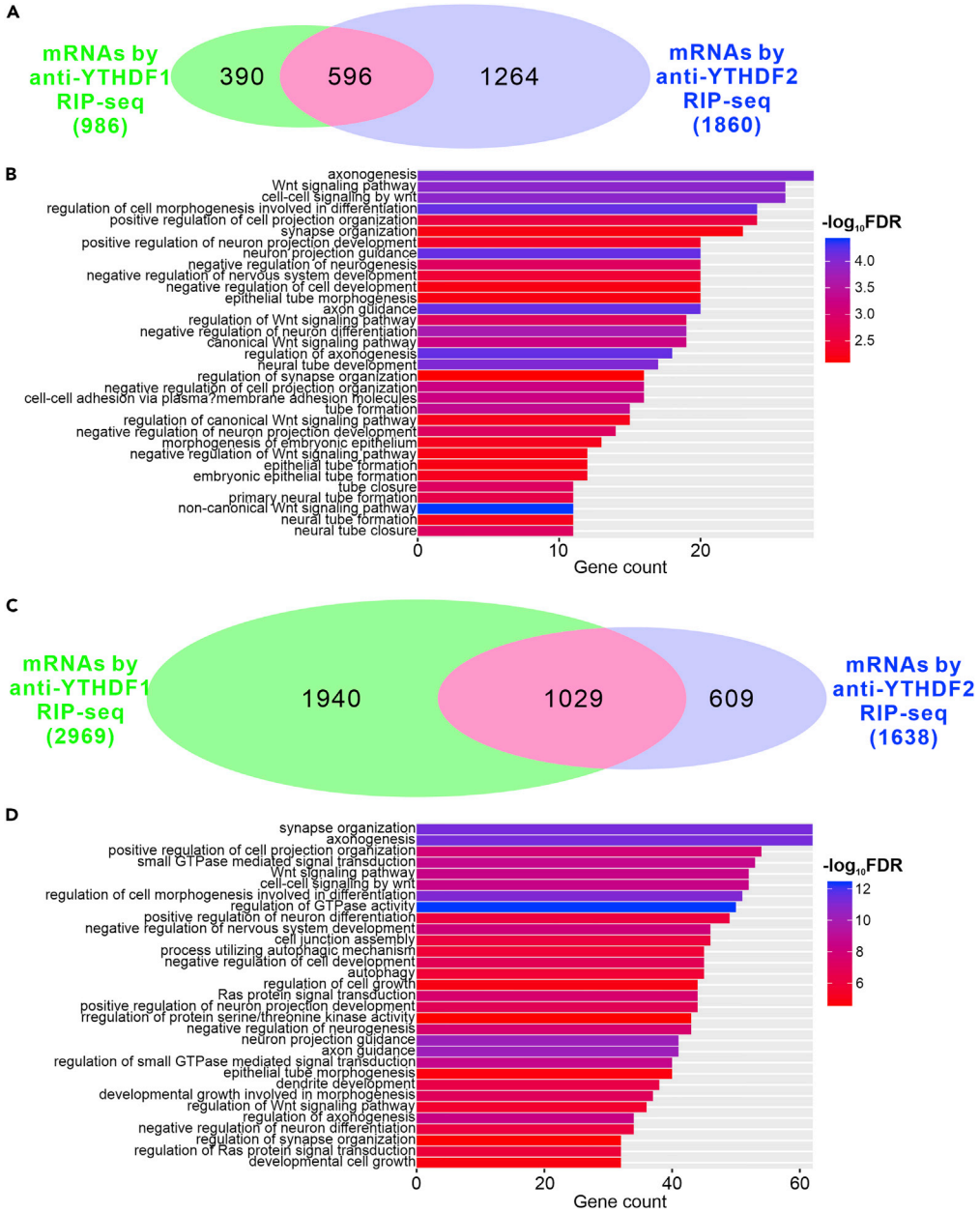

Figure 7. YTHDF1 and YTHDF2 share a large pool of target mRNAs related to neurogenesis in mouse cortex and retina

(A) Venn diagram showing numbers of mRNAs identified by anti-YTHDF1 and anti-YTHDF2 RNA immunoprecipitation followed by RNA sequencing (RIP-seq) in wildtype E12.5 cortex.

(B) Gene ontology (GO) analysis of overlapping target mRNAs of YTHDF1 and YTHDF2 in cortex. The GO terms in Biological Process are shown.

(C) Venn diagram showing numbers of mRNAs identified by anti-YTHDF1 and anti-YTHDF2 RIP-seq in wildtype P0 retina.

(D) GO analysis of overlapping target mRNAs of YTHDF1 and YTHDF2 in retina. The GO terms in Biological Process are shown.

This functional redundancy of YTHDFs seems to have tissue-specificity because double conditional knockout of *Ythdf1* and *Ythdf2* can recapitulate the phenotypes of *Mettl14* conditional knockout in cortex, whereas only triple conditional knockout of *Ythdf1*, *Ythdf2* and *Ythdf3* can reproduce those of *Mettl14* conditional knockout in retina. Further studies might be needed to explain this tissue-specificity.

Although YTHDFs are redundant in mediating m^{6}A modification in neurogenesis, they have unique and specific roles in postmitotic neurons. Conditional knockout of *Ythdf1* or *Ythdf2* in cerebellar granule cells (GC) promoted GC axon growth because YTHDF1 and YTHDF2 can synergistically regulate Wnt5a/PCP pathway through controlling local translation of *Dvl1* and *Wnt5a*, respectively (Yu et al., 2021). Conditional knockout of *Ythdf1* in dorsal spinal commissural neurons impaired translation of *Robo3.1* mRNA, and disturbed commissural axon guidance (Zhuang et al., 2019). Conditional knockout of *Ythdf2* in retinal ganglion cells (RGCs) increased RGC dendrite branching and improved visual acuity (Niu et al., 2022). Thus, the m^{6}A readers YTHDFs have sequential functions in neuronal development, initially mediating m^{6}A modification in neurogenesis redundantly, and then exerting unique and specific roles to regulate axon and dendrite development of postmitotic neurons.

Limitations of the study

Our current study demonstrates that the functionally redundant YTHDFs mediate m^{6}A regulation of cortical and retinal neurogenesis. We found that *Ythdf1* and *Ythdf2* double deletion, or only *Ythdf1*, *Ythdf2*, and *Ythdf3* triple deletion recapitulates the phenotype of *Mettl14* knockout in cortical or retinal neurogenesis, respectively. In addition, we identified a few target mRNAs which might be the driver targets mediating the redundant functions of YTHDFs in neurogenesis. However, further mechanistic studies are needed to elucidate the tissue-specificity of the YTHDFs redundancy, and the functions of the YTHDFs targets in neurogenesis.

STAR★METHODS

Detailed methods are provided in the online version of this paper and include the following:

- KEY RESOURCES TABLE
- RESOURCE AVAILABILITY
  - Lead contact
  - Materials availability
  - Data and code availability
- EXPERIMENTAL MODEL AND SUBJECT DETAILS
  - Animals
- METHOD DETAILS
  - Immunofluorescence and immunostaining
  - *In situ* hybridization (ISH)
  - BrdU assay
  - RNA immunoprecipitation and sequencing (RIP-seq)
  - RT-qPCR assay
- QUANTIFICATION AND STATISTICAL ANALYSIS
  - Statistical analysis

SUPPLEMENTAL INFORMATION

Supplemental information can be found online at https://doi.org/10.1016/j.isci.2022.104908.

ACKNOWLEDGMENTS

We thank Yuxi Sun and Jianhui Liu for technical assistance, and other members of Ji and Ou laboratories for help, technical support, and comments on the manuscript.

This work was supported by National Natural Science Foundation of China (32170955 and 31871038 to S.-J.J.), Shenzhen-Hong Kong Institute of Brain Science-Shenzhen Fundamental Research Institutions (2022SHIBS0002), High-Level University Construction Fund for Department of Biology (internal grant no. G02226301), Science and Technology Innovation Commission of Shenzhen Municipal Government (ZDSYS20200811144002008).

AUTHOR CONTRIBUTIONS

Conceptualization: S.J.J., F.N., and P.C.; Methodology: F.N., P.C., Z.Y., and X.O.; Validation: F.N., P.C., Z.Y., and S.J.J.; Formal analysis: F.N., P.C., Z.Y., and L.Y.; Investigation: F.N., P.C., Z.Y., M.Z., J.Z., L.Y.,

X.O., and S.J.J.; Data curation: F.N. and P.C.; Writing - review & editing: F.N. and S.J.J.; Visualization: F.N. and P.C.; Supervision: S.J.J. and X.O.; Project administration: S.J.J.; Funding acquisition: S.J.J.

DECLARATION OF INTERESTS

The authors declare no competing interests.

Received: May 3, 2022
Revised: July 12, 2022
Accepted: August 5, 2022
Published: September 16, 2022

REFERENCES

Anders, S., Pyl, P.T., and Huber, W. (2015). HTSeq–a Python framework to work with high-throughput sequencing data. Bioinformatics *31*, 166–169.

Brodie-Kommit, J., Clark, B.S., Shi, Q., Shiau, F., Kim, D.W., Langel, J., Sheely, C., Ruzycki, P.A., Fries, M., Javed, A., et al. (2021). Atoh7-independent specification of retinal ganglion cell identity. Sci. Adv. *7*, eabe4983.

Cepko, C. (2014). Intrinsically different retinal progenitor cells produce specific types of progeny. Nat. Rev. Neurosci. *15*, 615–627.

Dobin, A., Davis, C.A., Schlesinger, F., Drenkow, J., Zaleski, C., Jha, S., Batut, P., Chaisson, M., and Gingeras, T.R. (2013). STAR: ultrafast universal RNA-seq aligner. Bioinformatics *29*, 15–21.

Fishell, G., and Kriegstein, A.R. (2003). Neurons from radial glia: the consequences of asymmetric inheritance. Curr. Opin. Neurobiol. *13*, 34–41.

Furuta, Y., Lagutin, O., Hogan, B.L., and Oliver, G.C. (2000). Retina- and ventral forebrain-specific Cre recombinase activity in transgenic mice. Genesis *26*, 130–132.

He, P.C., and He, C. (2021). m(6) A RNA methylation: from mechanisms to therapeutic potential. EMBO J. *40*, e105977.

Hicks, E.A., Zaveri, M., Deschamps, P.A., Noseworthy, M.D., Ball, A., Williams, T., and West-Mays, J.A. (2018). Conditional deletion of AP-2α and AP-2β in the developing murine retina leads to altered amacrine cell mosaics and disrupted visual function. Invest. Ophthalmol. Vis. Sci. *59*, 2229–2239.

Huang, H., Zhang, G., Ruan, G.X., Li, Y., Chen, W., Zou, J., Zhang, R., Wang, J., Ji, S.J., Xu, S., and Ou, X. (2022). Mettl14-Mediated m6A modification is essential for germinal center B cell response. J. Immunol. *208*, 1924–1936.

Ji, S.J., Periz, G., and Sockanathan, S. (2009). Nolz1 is induced by retinoid signals and controls motoneuron subtype identity through distinct repressor activities. Development *136*, 231–240.

Kontur, C., Jeong, M., Cifuentes, D., and Giraldez, A.J. (2020). Ythdf m(6)A readers function redundantly during zebrafish development. Cell Rep. *33*, 108598.

Krishnaswamy, A., Yamagata, M., Duan, X., Hong, Y.K., and Sanes, J.R. (2015). Sidekick 2 directs formation of a retinal circuit that detects differential motion. Nature *524*, 466–470.

Lasman, L., Krupalnik, V., Viukov, S., Mor, N., Aguilera-Castrejon, A., Schneir, D., Bayerl, J., Mizrahi, O., Peles, S., Tawil, S., et al. (2020). Context-dependent functional compensation between Ythdf m(6)A reader proteins. Genes Dev. *34*, 1373–1391.

Li, Y., Li, H., Zhang, L., Xiong, S., Wen, S., Xia, X., and Zhou, X. (2019). Growth/differentiation 5 promotes the differentiation of retinal stem cells into neurons via Atoh8. J. Cell. Physiol. *234*, 21307–21315.

Lu, Q., Ivanova, E., Ganjawala, T.H., and Pan, Z.H. (2013). Cre-mediated recombination efficiency and transgene expression patterns of three retinal bipolar cell-expressing Cre transgenic mouse lines. Mol. Vis. *19*, 1310–1320.

Luo, H., Jin, K., Xie, Z., Qiu, F., Li, S., Zou, M., Cai, L., Hozumi, K., Shima, D.T., and Xiang, M. (2012). Forkhead box N4 (Foxn4) activates Dll4-Notch signaling to suppress photoreceptor cell fates of early retinal progenitors. Proc. Natl. Acad. Sci. USA *109*, E553–E562.

Meyer, K.D., and Jaffrey, S.R. (2017). Rethinking m(6)A readers, writers, and erasers. Annu. Rev. Cell Dev. Biol. *33*, 319–342.

Moffat, J.J., Jung, E.M., Ka, M., Smith, A.L., Jeon, B.T., Santen, G.W.E., and Kim, W.Y. (2019). The role of ARID1B, a BAF chromatin remodeling complex subunit, in neural development and behavior. Prog. Neuro-Psychopharmacol. Biol. Psychiatry *89*, 30–38.

Moffat, J.J., Jung, E.M., Ka, M., Jeon, B.T., Lee, H., and Kim, W.Y. (2021). Differential roles of ARID1B in excitatory and inhibitory neural progenitors in the developing cortex. Sci. Rep. *11*, 3856.

Niu, F., Han, P., Zhang, J., She, Y., Yang, L., Yu, J., Zhuang, M., Tang, K., Shi, Y., Yang, B., et al. (2022). The m(6)A reader YTHDF2 is a negative regulator for dendrite development and maintenance of retinal ganglion cells. Elife *11*, e75827.

Sapkota, D., Chintala, H., Wu, F., Fliesler, S.J., Hu, Z., and Mu, X. (2014). Onecut1 and Onecut2 redundantly regulate early retinal cell fates during development. Proc. Natl. Acad. Sci. USA *111*, E4086–E4095.

Schindelin, J., Arganda-Carreras, I., Frise, E., Kaynig, V., Longair, M., Pietzsch, T., Preibisch, S., Rueden, C., Saalfeld, S., Schmid, B., et al. (2012). Fiji: an open-source platform for biological-image analysis. Nat. Methods *9*, 676–682.

Shi, H., Wang, X., Lu, Z., Zhao, B.S., Ma, H., Hsu, P.J., Liu, C., and He, C. (2017). YTHDF3 facilitates translation and decay of N6-methyladenosine-modified RNA. Cell Res. *27*, 315–328.

Wang, X., Lu, Z., Gomez, A., Hon, G.C., Yue, Y., Han, D., Fu, Y., Parisien, M., Dai, Q., Jia, G., et al. (2014). N6-methyladenosine-dependent regulation of messenger RNA stability. Nature *505*, 117–120.

Wang, B., Balakrishnan-Renuka, A., Napirei, M., Theiss, C., and Brand-Saberi, B. (2015a). Spatiotemporal expression of Math6 during mouse embryonic development. Histochem. Cell Biol. *143*, 575–582.

Wang, X., Zhao, B.S., Roundtree, I.A., Lu, Z., Han, D., Ma, H., Weng, X., Chen, K., Shi, H., and He, C. (2015b). N(6)-methyladenosine modulates messenger RNA translation efficiency. Cell *161*, 1388–1399.

Wang, Y., Li, Y., Yue, M., Wang, J., Kumar, S., Wechsler-Reya, R.J., Zhang, Z., Ogawa, Y., Kellis, M., Duester, G., and Zhao, J.C. (2018). N(6)-methyladenosine RNA modification regulates embryonic neural stem cell self-renewal through histone modifications. Nat. Neurosci. *21*, 195–206.

Woodworth, M.B., Greig, L.C., Kriegstein, A.R., and Macklis, J.D. (2012). SnapShot: cortical development. Cell *151*, 918–918.e1.

Wu, H., Fan, J., Zhu, L., Liu, S., Wu, Y., Zhao, T., Wu, Y., Ding, X., Fan, W., and Fan, M. (2009). Sema4C expression in neural stem/progenitor cells and in adult neurogenesis induced by cerebral ischemia. J. Mol. Neurosci. *39*, 27–39.

Yang, Q.Q., Zhai, Y.Q., Wang, H.F., Cai, Y.C., Ma, X.Y., Yin, Y.Q., Li, Y.D., Zhou, G.M., Zhang, X., Hu, G., and Zhou, J.W. (2021). Nuclear isoform of FGF13 regulates post-natal neurogenesis in the hippocampus through an epigenomic mechanism. Cell Rep. *35*, 109127.

Yoon, K.J., Ringeling, F.R., Vissers, C., Jacob, F., Pokrass, M., Jimenez-Cyrus, D., Su, Y., Kim, N.S., Zhu, Y., Zheng, L., et al. (2017). Temporal control of mammalian cortical neurogenesis by m6A methylation. Cell *171*, 877–889.e17.

Yu, J., She, Y., Yang, L., Zhuang, M., Han, P., Liu, J., Lin, X., Wang, N., Chen, M., Jiang, C., et al. (2021). The m(6) A readers YTHDF1 and YTHDF2 synergistically control cerebellar parallel fiber growth by regulating local translation of the key Wnt5a signaling components in axons. Adv. Sci. *8*, e2101329.

Zaccara, S., and Jaffrey, S.R. (2020). A unified model for the function of YTHDF proteins in regulating m(6)A-modified mRNA. Cell *181*, 1582–1595.e18.

Zaccara, S., Ries, R.J., and Jaffrey, S.R. (2019). Reading, writing and erasing mRNA methylation. Nat. Rev. Mol. Cell Biol. *20*, 608–624.

Zhuang, M., Li, X., Zhu, J., Zhang, J., Niu, F., Liang, F., Chen, M., Li, D., Han, P., and Ji, S.J. (2019). The m6A reader YTHDF1 regulates axon guidance through translational control of Robo3.1 expression. Nucleic Acids Res. *47*, 4765–4777.

STAR★METHODS

KEY RESOURCES TABLE

REAGENT or RESOURCE	SOURCE	IDENTIFIER
Antibodies		
Rabbit polyclonal anti-YTHDF1	Proteintech	Cat#: 17479-1-AP; RRID: AB_2217473
Rabbit polyclonal anti-YTHDF2	Proteintech	Cat#: 24744-1-AP; RRID: AB_2687435
Rabbit polyclonal anti-Mettl14	Sigma-Aldrich	Cat#: HPA038002; RRID: AB_10672401
Rabbit polyclonal anti m^6A	Synaptic Systems	Cat# 202003; RRID: AB_2279214
Mouse monoclonal anti-Pax6	BD Biosciences	Cat#: 561462; RRID: AB_10715442
Rat monoclonal anti-BrdU	Abcam	Cat#: ab6326; RRID: AB_305426
Rabbit monoclonal anti-Ki67	Cell Signaling	Cat#: 12202S; RRID: AB_2620142
Rabbit polyclonal anti-Tbr1	Abcam	Cat#: ab31940; RRID: AB_2200219
Rat monoclonal anti-Ctip2	Abcam	Cat#: ab18465; RRID: AB_2064130
Rabbit monoclonal anti-Tbr2	Abcam	Cat#: ab183991; RRID: AB_2721040
Mouse monoclonal anti-AP2α	DSHB	Cat#: 3B5; RRID: AB_2313947
Mouse monoclonal anti-Brn3a	Millipore	Cat#: MAB1585; RRID: AB_94166
Rabbit polyclonal anti-PKCα	Cell Signaling	Cat#: CST-2056
Guinea pig polyclonal anti-Isl1/2	(Ji et al., 2009)	N/A
Sheep polyclonal anti-Chx10	Exalpha	Cat#: X1179P; RRID: AB_2889828
Alexa 488 donkey anti-g. pig IgG	Jackson Immunoresearch	Cat#: 706-545-148; RRID: AB_2340472
Alexa 488 donkey anti-mouse IgG	Thermo Fisher Scientific	Cat#: A-21202; RRID: AB_141607
Alexa 488 donkey anti-rabbit IgG	Thermo Fisher Scientific	Cat#: A-21206; RRID: AB_141708
Alexa 488 donkey anti-rat IgG	Thermo Fisher Scientific	Cat#: A-21208; RRID: AB_2535794
Alexa 555 donkey anti-mouse IgG	Thermo Fisher Scientific	Cat#: A-31570; RRID: AB_2536180
Alexa 555 donkey anti-rabbit IgG	Thermo Fisher Scientific	Cat#: A-31572; RRID: AB_162543
Alexa 555 donkey anti-sheep IgG	Thermo Fisher Scientific	Cat# A-21436; RRID: AB_2535857
Alexa 647 donkey anti-mouse IgG	Thermo Fisher Scientific	Cat#: A-31571; RRID: AB_162542
Critical commercial assays		
EZ-Magna RIP™ RNA-Binding Protein Immunoprecipitation Kit	Millipore	Cat#: 17-701
Experimental models: Organisms/strains		
Mouse: $Mettl14^{fl/fl}$	(Huang et al., 2022)	N/A
Mouse: $Ythdf1^{fl/fl}$	(Zhuang et al., 2019)	N/A
Mouse: $Ythdf2^{fl/fl}$	(Yu et al., 2021)	N/A
Mouse: $Ythdf3^{fl/fl}$	This paper	N/A
Mouse: Tg(Nes-cre)1Kln/J	Jackson Laboratory	Cat#: JAX_003771
Mouse: Tg(Six3-cre)69Frty/GcoJ	Jackson Laboratory	Cat#: JAX_019755
Oligonucleotides		
ISH Probe primers of mouse *Ythdf3*: Fwd: TGCTCCGTCCATTGGATT Rev: CGAGGAGCTACCCAACGA	This paper	N/A
qPCR primers of mouse *Gapdh* Fwd: TTGTCAGCAATGCATCCTGCACCACC Rev: CTGAGTGGCAGTGATGGCATGGAC	(Niu et al., 2022)	N/A

(*Continued on next page*)

Continued

REAGENT or RESOURCE	SOURCE	IDENTIFIER
qPCR primers of mouse *Ythdf1* Fwd: GGACAGTCCAATCCGAGTAACA Rev: CCTCGCTGAGGGAGTAAGGA	This paper	N/A
qPCR primers of mouse *Ythdf2*: Fwd: GAGCAGAGACCAAAAGGTCAAG Rev: CTGTGGGCTCAAGTAAGGTTC	(Niu et al., 2022)	N/A
qPCR primers of mouse *Ythdf3*: Fwd: GCCATGCGAAGGGAGAGAAA Rev: AGGCATTTCCAGAGTCTACATCAAG	This paper	N/A
qPCR primers of mouse *Arid1b*: Fwd: CCGATGGACCCAATGGTGATG Rev: TGGCCTTGCTGGCAGTAGCC	(Yang et al., 2021)	N/A
qPCR primers of mouse *Atoh8*: Fwd: AGCCAAGAAACGGAAGGAGTGAC Rev: TGGCAGCATCTTGAGGAAGAC	This paper	N/A
qPCR primers of mouse *Sema4c*: Fwd: ACCCCAGCCTAGGCCCC Rev: CAGGGGATGCCCACAAATGA	This paper	N/A
Mouse genotyping primers for *Mettl14loxP* site 1: CTGCCTGAACCTCTTGAGAACTGA and GCAGACAAGTGAGGAAATAAGCAAG	This paper	N/A
Mouse genotyping primers for *Mettl14loxP* site 2: GGAGGTGAACCTGATGAGCATT and CAACTGTAAGTGGCCGCTGGA	This paper	N/A
Mouse genotyping primers for *Ythdf1loxP* site 1: TAGTGCATTGTTAAGGCTGTCCTCGT and CTGCTGTCTCAAAGCACAAAGCCT	(Zhuang et al., 2019)	N/A
Mouse genotyping primers for *Ythdf1loxP* site 2: CTTAGAAATCAGTGTTTGTGGCCCA and CCTGCCTCAACACACCATTCTCTTT	(Zhuang et al., 2019)	N/A
Mouse genotyping primers for *Ythdf2loxP* site 1: GCTTGTAGTTATGTTGTGTACCAC and GCAGCTCTGACTATTCTAAAACCTCC	(Niu et al., 2022)	N/A
Mouse genotyping primers for *Ythdf2loxP* site 2: CTCATAACATCCATAGCCACAGG and CCAAGAGATAGCTTTCCTAATG	(Niu et al., 2022)	N/A
Mouse genotyping primers for *Ythdf3loxP* site 1: CAAACCAGAACAACGTAAGGCC and CTGGGTATGAAGCCCCACTGAT	This paper	N/A
Mouse genotyping primers for *Ythdf3loxP* site 2: ATTCCTTGCATGCTGTTCTAAAGT and AGTTCATATATAGAGCTGGAGAGC	This paper	N/A
Mouse genotyping primers for *Nestin-cre*: TTGCTAAAGCGCTACATAGGA (WT F) and CCTTCCTGAAGCAGTAGAGCA (Mut F) and GCCTTATTGTGGAAGGACTG (Common R)	This paper	N/A
Mouse genotyping primers for *Six3-cre*: CCTTCCTCCCTCTCTATGTG and GAACGAACCTGGTCGAAATC	(Niu et al., 2022)	N/A

(*Continued on next page*)

Continued

REAGENT or RESOURCE	SOURCE	IDENTIFIER
Software and algorithms		
GraphPad Prism 9.0	GraphPad	https://www.graphpad.com; RRID: SCR_002798
ImageJ (Fiji)	(Schindelin et al., 2012)	http://fiji.sc; RRID:SCR_002285
STAR v2.5	(Dobin et al., 2013)	https://github.com/alexdobin/STAR/
HTSeq	(Anders et al., 2015)	https://pypi.org/project/HTSeq/

RESOURCE AVAILABILITY

Lead contact

Further information and requests for resources and reagents should be directed to and will be fulfilled by the lead contact, Sheng-Jian Ji (jisj@sustech.edu.cn).

Materials availability

This study did not generate new unique reagents.

Data and code availability

The RIPseq data generated in this study has been deposited in GEO under accession number GSE199962. Other data reported in this paper will be shared by the lead contact upon request. This paper does not report original code. Any additional information required to reanalyze the data reported in this paper is available from the lead contact upon request.

EXPERIMENTAL MODEL AND SUBJECT DETAILS

Animals

Mettl14 $^{fl/fl}$, *Ythdf1*$^{fl/fl}$ and *Ythdf2*$^{fl/fl}$ mice were reported previously (Huang et al., 2022; Yu et al., 2021; Zhuang et al., 2019). For generation of *Ythdf3* conditional knockout mice, exon 3 of mouse *Ythdf3* was targeted and *loxP* sites were inserted flanking *Ythdf3* exon 3. *Nestin-cre* (The Jackson Laboratory, # 003,771) and *Six3-cre* (Furuta et al., 2000) (The Jackson Laboratory, # 019,755) were originally from The Jackson Laboratory. For timed pregnancy, embryos were identified as E0.5 when a copulatory plug was observed. Genotyping primers are as follows: the first *Mettl14*-loxp site: 5′-CTGCCTGAACCTCTTGAGAACTGA-3′ and 5′-GCAGACAAGTGAGGAAATAAGCAAG-3′; the second *Mettl14*-loxp site: 5′-GGAGGTGAACCTGAT GAGCATT-3′ and 5′-CAACTGTAAGTGGCCGCTGGA-3′. The first *Ythdf1*-loxp site: 5′-TAGTGCATTGTT AAGGCTGTCCTCGT-3′ and 5′-CTGCTGTCTCAAAGCACAAAGCCT-3′; the second *Ythdf1*-loxp site: 5′-CTTAGAAATCAGTGTTTGTGGCCCA-3′ and 5′-CCTGCCTCAACACACCATTCTCTTT-3′. The first *Ythdf2*-loxp site: 5′-GCTTGTAGTTATGTTGTGTACCAC-3′ and 5′-GCAGCTCTGACTATTCTAAAACCTC C-3′; the second *Ythdf2*-loxp site: 5′-CTCATAACATCCATAGCCACAGG-3′ and 5′-CCAAGAGATAG CTTTCCTAATG-3′. The first *Ythdf3*-loxp site: 5′-CAAACCAGAACAACGTAAGGCC-3′ and 5′-CTGGGTAT GAAGCCCCACTGAT-3′; the second *Ythdf3*-loxp site: 5′-ATTCCTTGCATGCTGTTCTAAAGT-3′ and 5′-AGTTCATATATAGAGCTGGAGAGC-3′. *Nestin-cre* site: 5′-CCTTCCTGAAGCAGTAGAGCA-3′ (Mut F) and 5′-GCCTTATTGTGGAAGGACTG-3′ (Common R) and 5′-TTGCTAAAGCGCTACATAGGA-3′ (WT F). *Six3-cre* site: 5′-CCTTCCTCCCTCTCTATGTG-3′ and 5′-GAACGAACCTGGTCGAAATC-3′. All experiments using mice were carried out following the animal protocols approved by the Laboratory Animal Welfare and Ethics Committee of Southern University of Science and Technology.

METHOD DETAILS

Immunofluorescence and immunostaining

For brain sections, mouse brain was dissected and fixed with 4% paraformaldehyde (Sigma) in 0.1 M Phosphate Buffer (PB) overnight at 4°C. After PBS washing, mouse brain was successively dehydrated with 15 and 30% sucrose in 0.1MPB for one day at 4°C, and then embedded with O.C.T. (SAKURA) and cryosectioned at 12 μm with Leica CM1950 Cryostat coronally. Coronal sections of brain were treated with sodium citrate buffer, pH 6.0 (Sigma) at 90°C for 40 min and then equilibrated at room temperature (RT). After PBS washing, brain sections were permeabilized and blocked with 10% donkey serum, 5% BSA (Sigma) and

0.25% Triton X-100 (Sigma) in PBS for 1 h at RT, and then incubated with 5% donkey serum, 5% BSA and 0.25% Triton X-100 in PBS overnight at 4°C with primary antibodies. After equilibrated at RT and three times of PBS washing, sections were incubated with 5% donkey serum, 5% BSA and 0.25% Triton X-100 in PBS for 2 h at RT with secondary antibodies. After two times of PBS washing, sections were mounted with the VECTASHIELD Antifade Mounting Medium with DAPI (Vector Laboratory).

For retinal vertical sections, E12.5 mouse embryos were fixed with 4% paraformaldehyde in 0.1MPB overnight at 4°C; embryonic eyes of later stages were fixed for 20–45 min at RT; eyes of mouse pups were pre-fixed briefly and then eyecups were dissected and fixed for 30–45 min at RT. After PBS washing, tissues were dehydrated with 30% sucrose in 0.1MPB overnight at 4°C, and then the E12.5 embryonic heads or the eyes of other stages were embedded with O.C.T. (SAKURA) and cryosectioned at 12 μm with Leica CM1950 Cryostat. Tissue sections were permeabilized and blocked with 1% BSA (Sigma) and 0.5% Triton X-100 (Sigma) in PBS (PBST) for 1 h at RT and incubated in PBST overnight at 4°C with primary antibodies. After three times of PBS washing, sections were incubated in PBST for 1 h at RT with secondary antibodies and then mounted with the VECTASHIELD Antifade Mounting Medium with DAPI (Vector Laboratory). METTL14 immunostaining experiments were carried out after antigen retrieval by sodium citrate buffer treatment.

Antibodies were used as follows: rabbit anti-YTHDF1 (1:1000, Proteintech 17479-1-AP), rabbit anti-YTHDF2 (1:1000, Proteintech 24744-1-AP), rabbit anti-METTL14 (1:1000, Sigma HPA038002), rabbit anti-m^{6}A (1:200, Synaptic Systems, 202,003), mouse anti-Pax6 (1:500, BD Biosciences 561,462), rat anti-BrdU (1:400, Abcam ab6326), rabbit anti-Ki67 (1:400, Cell Signaling 12202S), rabbit anti-Tbr1 (1:500, Abcam ab31940), rabbit anti-Tbr2 (1:500, Abcam ab183991), rat anti-Ctip2 (1:500, Abcam ab18465), mouse anti-AP2α (1:1000, DSHB 3B5), mouse anti-Brn3a (1:300, Millipore MAB1585), rabbit anti-PKCα (1:1000, Cell Signaling CST-2056), guinea pig anti-Isl1/2 (1:10,000) (Ji et al., 2009), sheep anti-Chx10 (1:1000, Exalpha X1179P); Alexa 488 donkey anti-guinea pig (1:500, Jackson 706-545-148), Alexa 488 donkey anti-mouse (1:500, Thermo A21202), Alexa 488 donkey anti-rabbit (1:500, Thermo A21206), Alexa 488 donkey anti-rat (1:500, Thermo A21208), Alexa 555 donkey anti-mouse (1:1000, Thermo A31570), Alexa 555 donkey anti-rabbit (1:1000, Thermo A31572), Alexa 555 donkey anti-sheep (1:1000, Thermo A21436), Alexa 647 donkey anti-mouse (1:200, Thermo A31571). All antibodies have been previously validated.

All images were captured on Nikon A1R confocal microscope, Zeiss LSM 800 confocal microscope or TissueGnostics TissueFAXS PLUS Upright Fluorescence and Brightfield System with identical settings for each group in the same experiment. The number of neurons in a specific area and the thickness of cortical layers were quantified blindly and manually.

In situ hybridization (ISH)

The PCR primers used for cloning mouse *Ythdf3* ISH probe are 5′-TGCTCCGTCCATTGGATT-3′ and 5′-CGAGGAGCTACCCAACGA-3′. The tissue sections for ISH were prepared as the immunofluorescence procedures with RNase-free reagents. Briefly, the tissue sections were fixed with 4% PFA in PBS and treated with Proteinase K. After re-fixation with PFA, the tissue sections were acetylated by acetic anhydride diluted in triethanolamine buffer. After acetylation, the prehybridization of sections were performed with the hybridization buffer for 2 h at 65°C and then the sections were hybridized with probes in fresh hybridization buffer overnight at 65°C. The sections were washed with preheated and RT 2× SSC sequentially, and then treated with 10 μg/mL RNase A in 2× SSC at 37°C for 8 min. After washing with 2× SSC, 0.2× SSC and PBT sequentially, the sections were blocked with 10% heat-inactivated sheep serum (SS) in PBT for 1 h at RT. Anti digoxygenin (Roche) was diluted in PBT with 10% SS, and used to incubate the sections overnight at 4°C. After washing with PBT and alkaline phosphatase buffer, NBT/BCIP (Roche) diluted in alkaline phosphatase buffer was used for color development reactions in darkness. After stopping color development reactions with PBS and briefly rinsing with ddH_2O, the sections were then mounted with Permount™ mounting medium. All images were captured on TissueGnostics TissueFAXS PLUS Upright Fluorescence and Brightfield System with identical settings for each group in the same experiment.

BrdU assay

BrdU dissolved in normal saline was injected in the E16.5 pregnant mice with 0.1 mg/g by intraperitoneal injection. The embryonic brains were collected 24 h after BrdU injection and treated as above. After antigen retrieval with sodium citrate buffer, the sections were treated with 2 M HCl at RT for 30 min and then 0.1 M

borate buffer at RT for 10 min. After PBS washing, the process of blocking and antibody incubation was performed as immunofluorescence and immunostaining.

RNA immunoprecipitation and sequencing (RIP-seq)

We used EZ-Magna RIP™ RNA-Binding Protein Immunoprecipitation Kit (Millipore) following the manual with minor modifications. $1 \times 10^7 \times 10^{12}$.5 cortical or P0 retinal neurons were lysed and incubated with YTHDF1 (Proteintech 17479-1-AP) or YTHDF2 antibody (Proteintech 24744-1-AP) overnight at 4°C. After quality control monitoring with Agilent 2100, 100 ng RNA of input and elutes after RIP were used to construct the libraries with TruSeq Stranded RNA Sample Preparation Kit (Illumina) and sequenced on the Illumina HiSeq 3000 platform (Jingneng, Shanghai, China). The filtered reads were then mapped to the mouse reference genome (GRCm38) using STAR v2.5 (Dobin et al., 2013) with default parameters. The resulting bam files were fed to HTSeq tool (Anders et al., 2015) to count the number of RNA-seq reads, which was further normalized to calculate FPKM. Any fold change greater than 2 of the FPKM from RIP elute to input was considered enriched. All enriched genes were used to do Gene Ontology (GO) analyses by the GOseq R package, in which gene length bias was corrected. GO terms with corrected p value less than 0.05 were considered significantly enriched.

RT-qPCR assay

RT-qPCR process was described previously (Niu et al., 2022). Total RNAs of *Ythdfs* cKO and control cortices or retinas were extracted by TRIzol Reagent (Life) and used for RT-qPCR. Primers used for qPCR are as following: mouse *Gapdh*: 5′-TTGTCAGCAATGCATCCTGCACCACC-3′ and 5′-CTGAGTGGCAGTGATG GCATGGAC-3′ (Niu et al., 2022); mouse *Ythdf1*: 5′-GGACAGTCCAATCCGAGTAACA-3′ and 5′-CCTCG CTGAGGGAGTAAGGA-3′; mouse *Ythdf2*: 5′-GAGCAGAGACCAAAAGGTCAAG-3′ and 5′-CTGTGGG CTCAAGTAAGGTTC-3′ (Niu et al., 2022); mouse *Ythdf3*: 5′-GCCATGCGAAGGGAGAGAAA-3′ and 5′-AG GCATTTCCAGAGTCTACATCA-3′; mouse *Arid1b*: 5′-CCGATGGACCCAATGGTGATG-3′ and 5′-TGG CCTTGCTGGCAGTAGCC-3′(Yang et al., 2021); mouse *Atoh8*: 5′-AGCCAAGAAACGGAAGGAGTGAC-3′ and 5′-TGGCAGCATCTTGAGGAAGAC-3′; mouse *Sema4c*: 5′-ACCCCAGCCTAGGCCCC-3′ and 5′-CA GGGGATGCCCACAAATGA-3′.

QUANTIFICATION AND STATISTICAL ANALYSIS

Statistical analysis

All experiments were conducted at a minimum of three independent biological replicates in the lab, and for cKO analysis, a minimum of three embryos/pups/mice were analyzed for each genotype. Statistical analysis was performed using GraphPad Prism 9.0. When comparing the means of two groups, an unpaired *t*-test was performed on the basis of experimental design. The settings for all box and whisker plots are: 25th-75th percentiles (boxes), minimum and maximum (whiskers), and medians (horizontal lines). The settings for all accumulative histograms are: mean (boxes), s.d. (stacked bars). A p value less than 0.05 was considered as statistically significant: *$p < 0.05$, **$p < 0.01$, ***$p < 0.001$, ****$p < 0.0001$.